^{191}Ir$(n, 2n)$ and ^{191}Ir$(n, 3n)$ reaction cross sections in the 15–21 MeV energy range

A. Kalamara,[1,*] R. Vlastou,[1] M. Kokkoris,[1] S. Chasapoglou,[1] A. Stamatopoulos,[1] N. Patronis,[2] M. Serris,[3] A. Lagoyannis,[4] and S. Harissopulos[4]

[1]*Department of Physics, National Technical University of Athens, 157 80 Athens, Greece*
[2]*Department of Physics, University of Ioannina, 451 10 Ioannina, Greece*
[3]*Department of Naval Architecture, University of West Attica, 122 10 Athens, Greece*
[4]*Institute of Nuclear and Particle Physics, NCSR "Demokritos", 153 10 Aghia Paraskevi, Greece*

(Received 12 June 2018; published 13 September 2018)

The cross sections of the ^{191}Ir$(n, 2n)^{190}$Ir and ^{191}Ir$(n, 3n)^{189}$Ir reactions have been determined by means of the activation technique, relative to the ^{27}Al$(n, \alpha)^{24}$Na reaction, at neutron beam energies higher than 15 MeV. The quasi-monoenergetic neutron beams were produced at the 5.5 MV Tandem T11/25 Accelerator Laboratory of NCSR "Demokritos" by implementing the ^{3}H$(d, n)^{4}$He reaction. The induced γ-ray activity of the irradiated target and reference foils was measured with high resolution, high purity germanium (HPGe) detectors. The cross section for the high-spin isomeric state (11^-) of the ^{190}Ir nucleus was determined along with the sum of the ground (4^-), the first (1^-), and the second (11^-) isomeric states. Moreover, the cross section for the production of the ground state of the residual nucleus of $(n, 3n)$ reaction, ^{189}Ir, was also estimated. Additionally, cross section theoretical calculations were carried out using the EMPIRE 3.2.2 and TALYS 1.8 codes, in which the input parameters were chosen in such a way as to simultaneously reproduce several experimental reaction channel cross sections in a satisfactory way, namely the $(n, 2n)$, $(n, 3n)$, (n, p), (n, α), and $(n,$ total) ones. Similar combination of theoretical model parameters had also been successfully used in the case of the neighboring ^{197}Au nucleus, and this constitutes an encouraging confirmation of how accurately the theoretical models can reproduce the experimental results in this mass region.

DOI: 10.1103/PhysRevC.98.034607

I. INTRODUCTION

Iridium is widely used in various medical and industrial applications. For example, as an activation detector it can probe the low and high energy components of the neutron fluence in neutron environments [1]. Especially the $(n, 2n)$ reaction products provide information on the high energy neutrons above the $(n, 2n)$ threshold, i.e., ∼9 MeV. More specifically, the reaction ^{191}Ir$(n, 2n)$ leads to the population of two levels of the residual nucleus ^{190}Ir which present large spin differences (isomeric state $m2$ has 11^- and ground state g has 4^-). Due to the existence of the former $(m2)$, the theoretical study of this reaction is a powerful tool for obtaining information on the structure of the involved nuclei and therefore constitutes an open field of study [2]. Above 15 MeV, apart from the energetically allowable $(n, 3n)$ competing reaction channel, an additional contribution to the cross section arises from the pree-quilibrium emission. Hence, the simultaneous reproduction of the isomeric cross section along with other channels sets a significant constraint, rendering theoretical calculations quite sensitive to the choice of specific nuclear model parameters such as the level density (α) and the spin cutoff (σ^2).

Regarding experimental measurements, six datasets [3–8] exist in literature [9] for the cross section of the sum of the ground and the first isomeric states $(g + m1)$, which present a few data points above 15 MeV, whereas for the cross section of the second metastable state $(m2)$, although there exist two datasets [5,10] in the energy range from 15 to 18 MeV, at higher energies there is a complete lack of experimental data. Moreover, the existence of accurate cross section values for the population of the high spin isomeric state, which has a much shorter half-life time ($m2$: $T_{1/2} = 3.25$ h) than the one of the ground state (g: $T_{1/2} = 11.78$ d), could give an important boost to experimental applications, since it offers the possibility of an immediate and less time-consuming activation analysis. Concerning the cross section of the $(n, 3n)$ reaction, only two datasets exist in the literature [4,11], therefore the present data can provide new information not only for the cross section libraries but also for the compound nucleus evaporation process when combined with the $(n, 2n)$ cross section data.

In 2007, the two $(n, 2n)$ reaction channels were studied by our group at four neutron beam energies between 10 and 11.3 MeV [7], and the present work constitutes a continuation of the previous one in order to determine the cross section at higher neutron energies, where the existing data are either sparse (in the case of the $g + m1$ cross section) or absent (in the case of the $m2$ cross section for energies above 18 MeV). At these energies, since the $(n, 3n)$ reaction channel is open, its cross section was studied and included in the present project.

For all the aforementioned reasons, the purpose of this work was to experimentally determine the ^{191}Ir$(n, 2n)^{190}$Ir, ^{191}Ir$(n, 2n)^{190}$Ir^{m2}, and ^{191}Ir$(n, 3n)^{189}$Ir reaction cross sections at incident neutron energies ranging from 15.3 to

*akalamara@central.ntua.gr

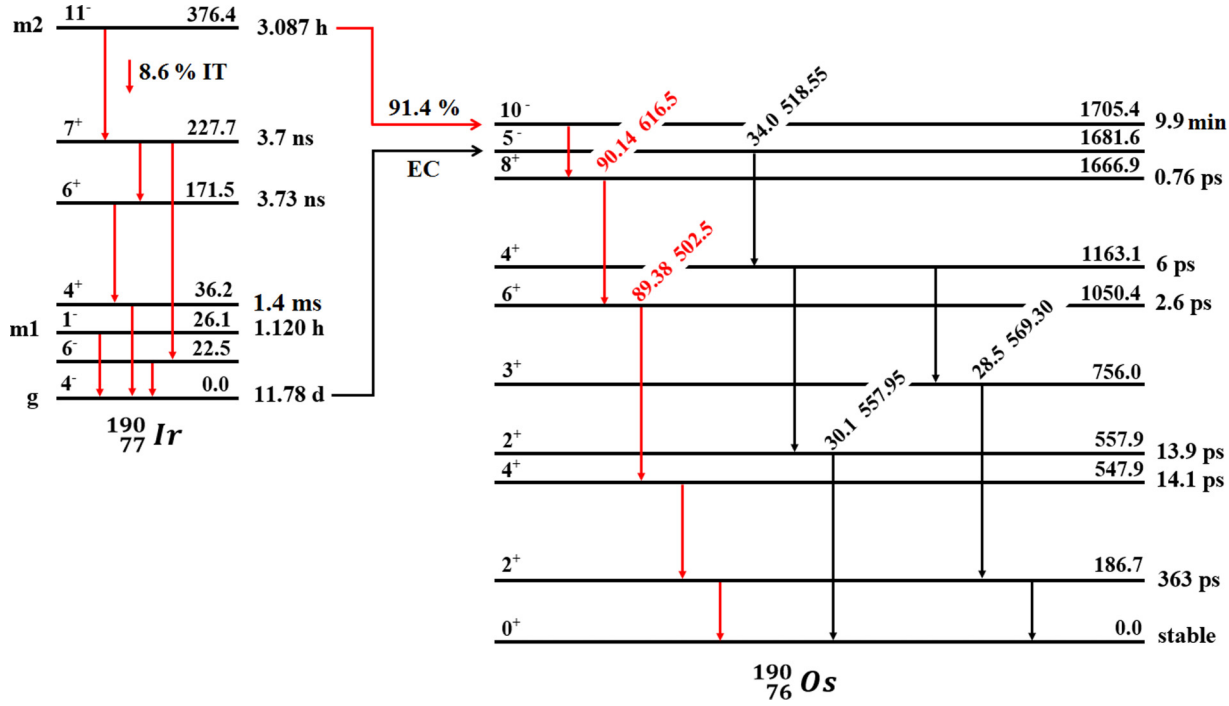

FIG. 1. Simplified decay scheme for the deexcitation of the ground and isomeric states of the ^{190}Ir nucleus. The intensities are obtained from the NNDC Brookhaven National Laboratory library [14] and from Refs. [15,16], and all energies are presented in keV.

20.9 MeV, implementing the activation technique. The ^{27}Al$(n,\alpha)^{24}$Na reaction was used as reference in order to determine the total neutron integrated fluence over the irradiation time. The irradiations were performed at the 5.5 MV Tandem T11/25 Accelerator Laboratory of NCSR "Demokritos" using quasi-monoenergetic neutrons produced by means of the ^{3}H$(d,n)^{4}$He reaction. Furthermore, theoretical statistical model calculations were performed over a wide energy range (10^{-8}–35 MeV) and the results were compared to all available experimental datasets in literature. Apart from the measured reactions, ^{191}Ir$(n,2n)^{190}$Ir, ^{191}Ir$(n,2n)^{190}$Ir^{m2}, and ^{191}Ir$(n,3n)^{189}$Ir, three more reaction channels have been simultaneously reproduced with the same parametrization, using the latest versions of EMPIRE and TALYS codes (3.2.2 [12] and 1.8 [13], respectively) and the obtained results are quite satisfactory.

II. THE RESIDUAL NUCLEI

A. The ^{190}Ir nucleus

The residual nucleus of the $(n,2n)$ reaction on ^{191}Ir, namely ^{190}Ir, is unstable and decays via electron capture (91.4%) and internal conversion (8.6%) to ^{190}Os (Fig. 1). The decay half-life of the ground state is 11.78 d and the deexcitation is accompanied by γ-ray emission, with the energies of the three most intense γ-rays being 518.55, 557.95, and 569.30 keV.

However, the nucleus can be produced at an excited state and populate one of the two isomeric states which lie at the excitation energies of 26.1 ($m1$) and 376.4 keV ($m2$), respectively. The former isomeric state decays with a half-life of 1.12 h by low energy γ-ray emission, and, due to the γ-ray high mass attenuation factor, its de-excitation cannot be easily studied. The latter, having a half-life of 3.087 h, decays to ^{190}Os with a probability of 91.4% and can be independently determined by measuring the two most intense γ rays (616.5 and 502.5 keV) emitted during its deexcitation.

Due to the fact that the 8.6% of the population of the $m2$ state decays to the ground state, the most appropriate summation to represent the experimental scenario in an activation measurement is given by the following expression [15]:

$$^{191}\mathrm{Ir}(n,2n)^{190}\mathrm{Ir}^{\,g+m1+0.086\,m2}$$

Thus, when measuring the 518.55, 557.95, and 569.30 keV γ-ray transitions, the population of the ground, first, and a part of second isomeric states is included in the results.

B. The ^{189}Ir nucleus

The residual nucleus of the $(n,3n)$ reaction on ^{191}Ir, namely ^{189}Ir, is unstable and decays by means of electron capture (100%) to ^{189}Os (Fig. 2) with a decay half-life 13.2 d. During its deexcitation several γ-rays are emitted; the most intense is the 245.1 keV one.

III. EXPERIMENTAL PROCEDURE

A. Activation

In order to determine the cross section of the ^{191}Ir$(n,2n)^{190}$Ir reaction, six irradiations were performed at the 5.5 MV Tandem T11/25 Accelerator Laboratory of NCSR "Demokritos" by means of the activation technique. The neutron beam energy was varied between 15.3 and 20.9 MeV, and the ^{27}Al$(n,\alpha)^{24}$Na reference reaction cross section was used in order to define the neutron flux during the irradiation.

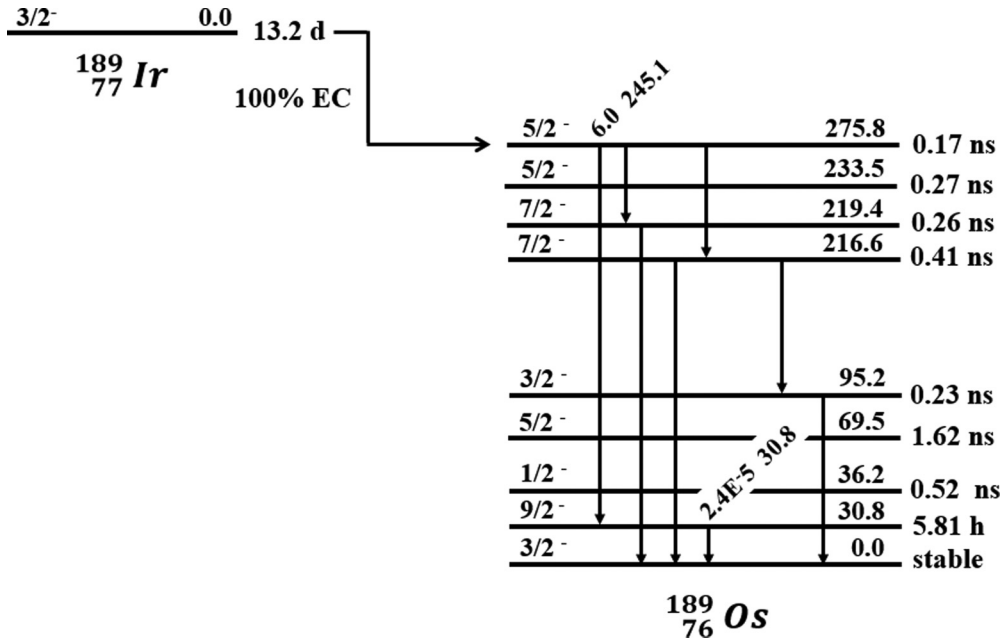

FIG. 2. Simplified decay scheme for the deexcitation of the ground state of the ^{189}Ir nucleus. The intensities are obtained from the NNDC Brookhaven National Laboratory library [14] and all energies are presented in keV.

The data obtained by the three irradiations with the longest irradiation time (see Table I) had sufficient statistics to allow for the determination of the cross section of the (n, 3n) reaction channel.

High purity Ir and Al foils (0.4–0.5 mm in thickness and 13–14 mm in diameter) were used for the measurements, while the Ir samples were stacked between two Al foils in order to accurately determine the neutron flux.

The quasi-monoenergetic neutron beams were produced by implementing the ^{3}H(d, n)^{4}He reaction (Q = 17.59 MeV) using a 0.2–1.5 μA deuterium beam which impinged on a solid Ti-tritiated target, as described in Refs. [17,18]. The distance of all the samples from the flange with the Ti-T target was ∼2 cm, thus limiting the angular acceptance to ±19°, where the neutron beam can practically be considered as monoenergetic. The flange with the Ti-T target assembly was air-cooled during the irradiation and the neutron fluence for each energy measurement is presented in Table I.

In order to record the neutron beam fluctuations during the irradiation time, which varied between 10 and 100 h (see Table I), a BF_3 detector was placed at a distance of 3 m from the neutron source. The beam instabilities were used in the offline analysis to correct for the decay of the product nuclei during the irradiation.

TABLE I. The neutron beam energy, the corresponding neutron fluence and the duration for each irradiation are presented.

E_n (MeV)	Duration (h)	Neutron flux (n/cm^2 s)
15.3 ± 0.5	26.1	(3.10 ± 0.12) × 10^6
17.1 ± 0.3	96.1	(2.24 ± 0.10) × 10^5
17.9 ± 0.3	9.7	(2.26 ± 0.10) × 10^5
18.9 ± 0.3	27.8	(3.02 ± 0.14) × 10^5
20.0 ± 0.2	10.1	(1.32 ± 0.10) × 10^5
20.9 ± 0.2	32.4	(2.43 ± 0.17) × 10^5

B. γ-ray spectroscopy

Following the end of the irradiations, the induced activity on the Ir target and reference foils was measured using three high purity germanium (HPGe) detectors of 100%, 56%, and 16% relative efficiency. The activity measurements of all samples were carried out at a distance of 10 cm from the detector window, thus there was no need for significant pile-up or true coincidence summing-effect corrections. At the same distance, a ^{152}Eu point source was placed in order to determine the absolute peak efficiency of each detector.

For the population of the second isomeric state ($m2$), the measurements began ∼1 h after the end of the irradiations and the corresponding cross sections were independently determined through the two most intense γ rays (616.5 and 518.55 keV) emitted during the deexcitation of the ^{190}Ir^{m2} nucleus [see Fig. 3(a)].

Apart from the aforementioned measurements, Ir spectra were also taken ∼2 d after the irradiations in order to obtain the cross section of the ground state, when the second metastable state ($T_{1/2}$ = 3.087 h) had fully decayed to the ground one. These cross section values were deduced as the weighted average using the integral of the 518.55, 557.95, and 569.30 keV γ-ray peaks and, as mentioned in Sec. II A, correspond to the sum of the population of ($g + m1 + 0.086\,m2$) levels. Typical spectra of iridium samples for the ($g + m1 + 0.086\,m2$) cross section are presented in Fig. 3(b), where the γ-ray peaks of interest have been marked.

Regarding the determination of the (n, 3n) reaction cross section, due to the half-life of 13.2 d, it is crucial to analyze

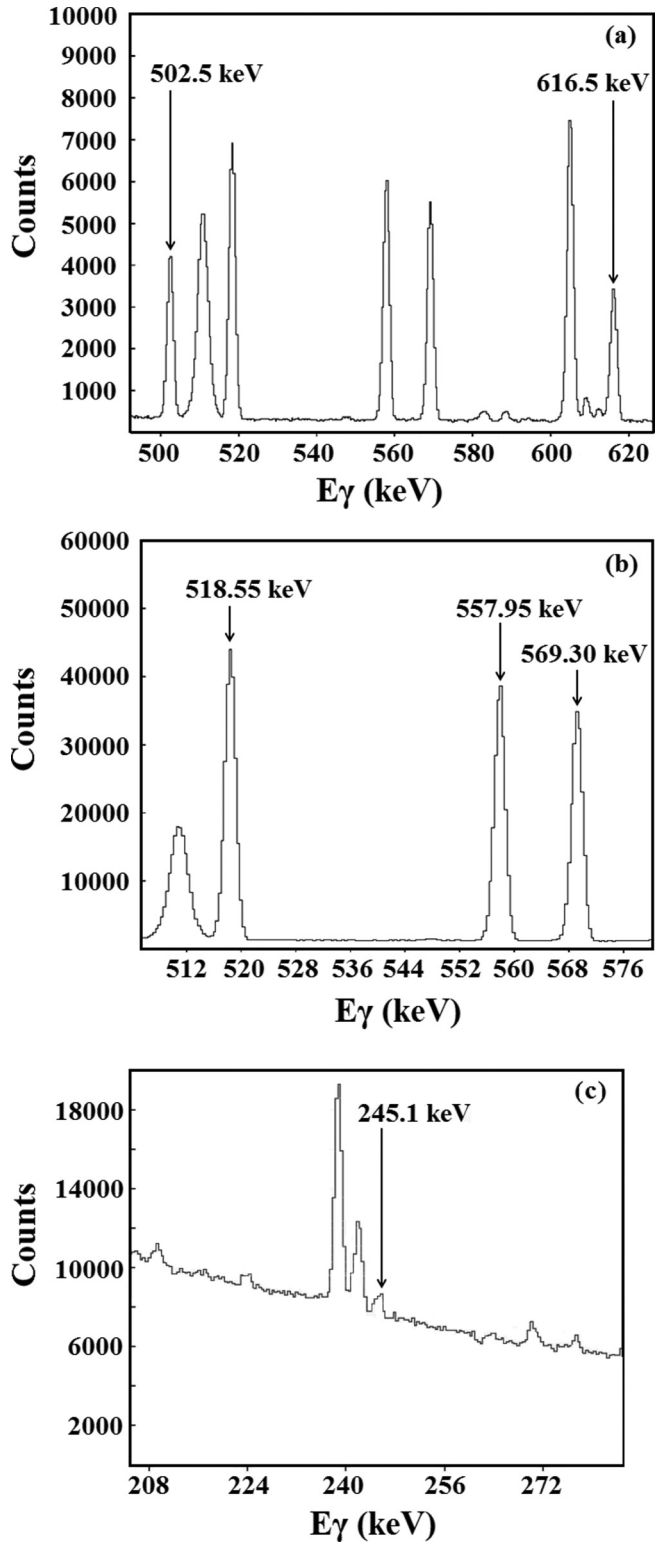

FIG. 3. Off-beam γ-ray energy spectra obtained after the neutron irradiation at 15.3 MeV [(a) and (b)]. γ-ray transitions from the decay of (a) the second isomeric ($m2$) of the ^{190}Ir nucleus and (b) the ground plus both isomeric states ($g + m1 + 0.086\,m2$) of the ^{190}Ir nucleus are marked. The durations of these measurements were 10 and 72 h, respectively. Concerning the measurement of the ground state of the ^{189}Ir nucleus (c), the 245.1 keV γ ray is marked in the 56 h spectrum obtained after the irradiation at 20.9 MeV.

TABLE II. Decay data used for the daughter nuclei [14].

Reaction	$T_{1/2}$	E_γ (keV)	I_γ (%)
^{191}Ir$(n, 2n)^{190}$Ir^{m2}	3.087 h	616.5	90.14
		502.5	89.38
^{191}Ir$(n, 2n)^{190}$Ir$^{g+m1+0.086\,m2}$	11.78 d	518.55	34.0
		557.95	30.1
		569.30	28.5
^{191}Ir$(n, 3n)^{189}$Ir	13.2 d	245.1	6.0
^{27}Al$(n, \alpha)^{24}$Na	14.997 h	1368.626	99.9936

spectra with the longest available duration, in order to collect more counts in the 245.1 keV γ peak integral [Fig. 3(c)].

The decay data of the reference and Ir targets are presented in Table II.

IV. ANALYSIS

In order to experimentally determine the cross section for the three measured reaction channels, the integral of the γ-ray peak in the spectrum obtained with the HPGe detector (N_γ), the absolute efficiency of the detector at the corresponding energy (ε_γ), the γ-ray intensity (I_γ), the number of the target nuclei (N_τ), and a correction factor for the γ-ray self-absorption effects (F) estimated via Monte Carlo simulations using the MCNP5 code [19], were combined according to the following expression:

$$\sigma_{\rm Ir} = \sigma_{\rm Al} \frac{N_{\gamma_{\rm Ir}}}{N_{\gamma_{\rm Al}}} \frac{(\varepsilon_\gamma I_\gamma F D f_c N_\tau)_{\rm Al}}{(\varepsilon_\gamma I_\gamma F D f_c N_\tau)_{\rm Ir}} C_\Phi. \quad (1)$$

An additional correction factor (D) was used for the counting collection,

$$D = e^{-\lambda t_1} - e^{-\lambda t_2}, \quad (2)$$

where λ is the decay constant of the residual nucleus and t_1, t_2 correspond to time intervals from the end of the irradiation to the beginning and end of the measurement with the HPGe detector, respectively. In order to correct for the produced nuclei which decayed during irradiation, the information on the beam fluctuations was taken into account through the following factor:

$$f_c = \frac{\int_0^{t_B} e^{\lambda t} f(t) dt}{\int_0^{t_B} f(t) dt} e^{-\lambda t_B} \quad (3)$$

where $f(t)$ are the counts obtained via the BF_3 counter, which represent the beam flux in arbitrary units over specific time intervals, and t_B is the duration of the irradiation in seconds. The cross section of the ^{27}Al$(n, \alpha)^{24}$Na reference reaction ($\sigma_{\rm Al}$) was adopted from the IRDFF 1.05 library [20], while the factor C_Φ corresponds to the neutron flux ratio in aluminum and iridium foils, and it was estimated both experimentally and with Monte Carlo simulations implementing MCNP5 [19]. Due to the fact that the agreement between experiment and simulation was very good, the uncertainty of the C_Φ factor was considered negligible.

TABLE III. Experimental cross section values and uncertainties for the ^{191}Ir$(n, 2n)^{190}$Ir^{m2}, ^{191}Ir$(n, 2n)^{190}$Ir$^{g+m1+0.086\,m2}$ and ^{191}Ir$(n, 3n)^{189}$Ir reactions.

E_n (MeV)	σ_{m2} (mb)	$\sigma_{g+m1+0.086\,m2}$ (mb)	$\sigma_{(n,3n)}$ (mb)
15.3 ± 0.5	179 ± 8	1786 ± 76	
17.1 ± 0.3	203 ± 15	1465 ± 72	167 ± 43
17.9 ± 0.3	210 ± 12	1291 ± 82	
18.9 ± 0.3	178 ± 10	991 ± 52	716 ± 179
20.0 ± 0.2	134 ± 13	731 ± 91	
20.9 ± 0.2	86 ± 7	479 ± 37	1095 ± 198

V. EXPERIMENTAL CROSS SECTIONS AND UNCERTAINTIES

The experimental results for the cross section of the three measured reaction channels ^{191}Ir$(n, 2n)^{190}$Ir^{m2}, ^{191}Ir$(n, 2n)^{190}$Ir$^{g+m1+0.086\,m2}$, and ^{191}Ir$(n, 3n)^{189}$Ir are presented in Table III along with their corresponding total estimated uncertainties. The $(n, 2n)$ cross section has been deduced for six neutron energies (see Table I), while the $(n, 3n)$ cross section could be extracted only at 17.1, 18.9 and 20.9 MeV, where the combination of the total neutron flux during irradiation and the cross section allowed for reasonable counting statistics.

In order to deduce the cross section of the second isomeric state, the weighted average of the cross sections obtained via the 616.5 and 502.5 keV γ rays was estimated, and the results are shown in Fig. 4 along with existing experimental datasets in literature. The results of the cross section of the sum of the $g + m1 + 0.086\,m2$, correspond to the weighted average of the cross sections deduced via the 518.55, the 557.95, and the 569.30 keV lines and are presented in Fig. 5 along with existing experimental datasets in literature and ENDF/B.VIII.0 evaluation results for the total $(n, 2n)$ channel. Concerning the $(n, 3n)$ reaction cross section, the experimental results were obtained only through one γ ray, namely the 245.1 keV one, since the other emitted ones could not be measured due to low counting statistics (see Fig. 6). All the experimental results are discussed in Sec. VII.

The most important uncertainties were evaluated and are presented in Table IV. Each of the six blocks of Table IV corresponds to the uncertainties and results of the cross sections obtained from each γ-ray line at every neutron energy. Due to the fact that all the factors involved in Eq. (1) were considered uncorrelated, the total uncertainties presented in the third

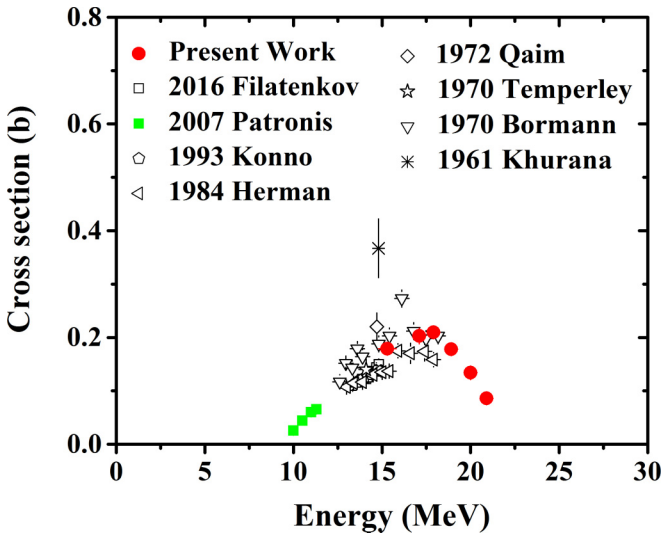

FIG. 4. Experimental cross section values for the ^{191}Ir$(n, 2n)^{190}$Ir^{m2} reaction compared with previous data.

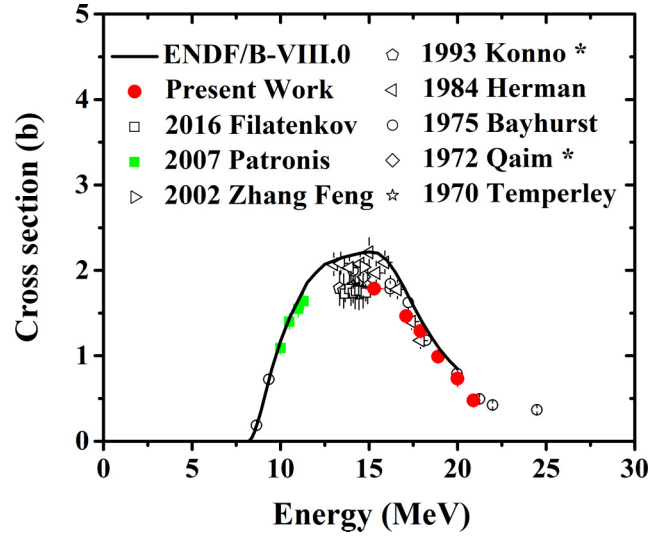

FIG. 5. Experimental cross section values for the ^{191}Ir$(n, 2n)^{190}$Ir$^{g+m1+0.086\,m2}$ reaction compared with previous data and ENDF/B-VIII.0 evaluation (solid curve). The datasets with an asterisk in the end correspond to the total $(n, 2n)$ channel cross section, while the rest correspond to $g + m1$ cross section values.

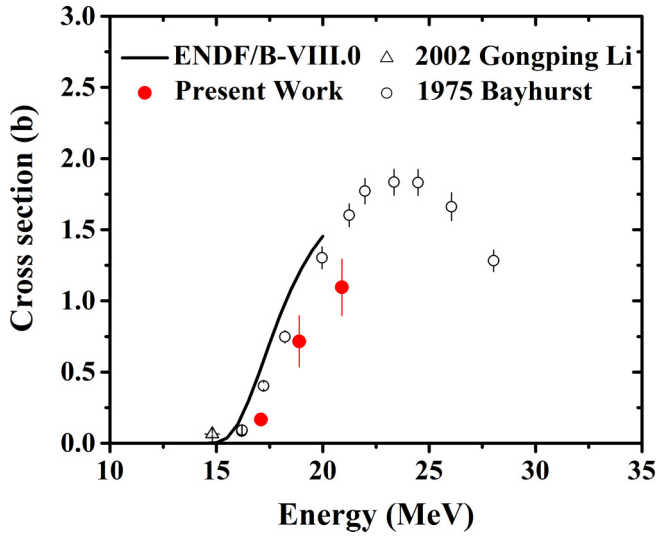

FIG. 6. Experimental cross section values for the ^{191}Ir$(n, 3n)^{189}$Ir reaction compared with previous data and ENDF/B-VIII.0 evaluation (solid curve).

TABLE IV. The ^{191}Ir$(n, 2n)^{190}$Ir^{m2}, ^{191}Ir$(n, 2n)^{190}$Ir$^{g+m1+0.086\,m2}$, and ^{191}Ir$(n, 3n)^{189}$Ir cross sections obtained from each γ ray (mentioned in Table III) along with the total uncertainties (in %) and the uncertainties for the most significant contributions in Eq. (1) at each neutron energy. The uncertainties of the $(N_\tau)_{\rm Ir}$ and $\sigma_{\rm Al}$ factors of Eq. (1) are the same for every row of the table (0.1% and 3% respectively), thus for convenience they are omitted from the table.

E_n	Cross section	Uncertainties (%)					
(MeV)	(b)	Total	$(N_\gamma)_{\rm Ir}$	$(N_\gamma)_{\rm Al}$	$(N_\tau)_{\rm Al}$	$(\varepsilon_\gamma)_{\rm Ir}$	$(\varepsilon_\gamma)_{\rm Al}$
	For ^{191}Ir$(n, 2n)^{190}$Ir^{m2} cross section obtained via the analysis of the 616.5 keV γ-ray peak						
15.3	0.176	4.9	1.8	0.3	0.5	2.5	2.3
17.1	0.196	9.9	8.5	2.3	0.6	2.5	2.4
17.9	0.211	6.7	4.3	1.6	0.5	2.8	2.7
18.9	0.182	5.8	2.4	1.2	0.6	2.8	3.1
20.0	0.131	11.3	7.0	2.1	0.5	5.3	6.2
20.9	0.084	9.4	3.4	0.9	0.5	5.3	6.2
	For ^{191}Ir$(n, 2n)^{190}$Ir^{m2} cross section obtained via the analysis of the 502.5 keV γ-ray peak						
15.3	0.182	4.9	1.8	0.3	0.5	2.6	2.3
17.1	0.210	8.9	7.2	2.3	0.6	2.6	2.4
17.9	0.208	7.2	5.0	1.6	0.5	2.9	2.7
18.9	0.172	6.5	3.7	1.2	0.6	2.9	3.1
20.0	0.138	11.2	6.7	2.1	0.5	5.3	6.2
20.9	0.089	9.6	3.9	0.9	0.5	5.3	6.2
	For ^{191}Ir$(n, 2n)^{190}$Ir$^{g+m1+0.086\,m2}$ cross section obtained via the analysis of the 518.55 keV γ-ray peak						
15.3	1.775	4.8	1.6	0.3	0.5	2.6	2.3
17.1	1.491	5.5	1.8	2.3	0.6	2.6	2.4
17.9	1.227	8.5	6.7	1.6	0.5	2.9	2.7
18.9	1.004	6.4	3.4	1.2	0.6	2.9	3.1
20.0	0.762	19.5	17.2	2.1	0.5	5.4	6.2
20.9	0.484	8.6	4.0	0.9	0.5	3.0	6.2
	For ^{191}Ir$(n, 2n)^{190}$Ir$^{g+m1+0.086\,m2}$ cross section obtained via the analysis of the 557.95 keV γ-ray peak						
15.3	1.780	4.9	1.6	0.3	0.5	2.6	2.3
17.1	1.421	5.3	1.1	2.3	0.6	2.6	2.4
17.9	1.398	8.7	7.0	1.6	0.5	2.9	2.7
18.9	0.980	6.2	3.1	1.2	0.6	2.9	3.1
20.0	0.777	17.5	15.0	2.1	0.5	5.4	6.2
20.9	0.467	9.0	4.9	0.9	0.5	3.0	6.2
	For ^{191}Ir$(n, 2n)^{190}$Ir$^{g+m1+0.086\,m2}$ cross section obtained via the analysis of the 569.30 keV γ-ray peak						
15.3	1.809	4.9	1.6	0.3	0.5	2.6	2.3
17.1	1.537	5.3	0.9	2.3	0.6	2.6	2.4
17.9	1.287	9.7	8.1	1.6	0.5	2.9	2.7
18.9	0.992	6.3	3.4	1.2	0.6	2.9	3.1
20.0	0.666	19.7	17.5	2.1	0.5	5.4	6.2
20.9	0.488	8.9	4.6	0.9	0.5	3.0	6.2
	For ^{191}Ir$(n, 3n)^{189}$Ir cross section obtained via the analysis of the 245.1 keV γ-ray peak						
17.1	0.167	25.7	25.0	2.3	0.6	3.6	2.4
18.9	0.716	25.0	24.2	1.2	0.6	4.3	3.1
20.9	1.095	18.1	14.8	0.9	0.5	7.8	6.2

column of Table IV have been deduced by a quadratical summation of all the uncertainties that exist in the same row of the table. Nevertheless, the correlations between the cross section measurements for the second isomeric state ($m2$) obtained from two γ-rays were taken into account by determining the weighted average according to Eq. (27) reported in Ref. [21]. Furthermore, in order to take into account the correlations in the case of the $(g + m1 + 0.086\,m2)$ cross sections, where the weighted averages were obtained from three γ rays and three cross section values, the formalism mentioned in Appendix 2 of [22] was adopted.

VI. THEORETICAL CALCULATIONS

Theoretical cross section calculations were performed for incident neutron energies ranging from 10^{-8} to 35 MeV, by

TABLE V. Basic keywords and the corresponding values used in the input file of the EMPIRE 3.2.2 code.

Keyword	Value
LEVDEN	0
DIRECT	0
HRTW	3
GSTRFN	1
OMPOT (n)	401
OMPOT (p)	5405
OMPOT (α)	9600
PCROSS	2.99

means of two nuclear reaction model codes, namely EMPIRE 3.2.2 [12,23] and TALYS 1.8 [13,24]. The purpose of this work was to determine the optimum combination of nuclear model parameters for each code and to achieve a good reproduction of the cross section for the three measured reaction channels [$(n, 2n)_{g+m1+0.086\,m2}$, $(n, 2n)_{m2}$, and $(n, 3n)$] and for three more: (n, p), (n, α), and $(n,$ total). In both codes, the compound nucleus reaction cross sections were calculated in the framework of the Hauser-Feshbach theory [25].

The basic keywords used in the input file of the EMPIRE code are presented in Table V. The description of the compound nucleus level densities was made by using the formalism of the enhanced generalized superfluid model (EGSM) [26], while the transmission coefficients were calculated by implementing optical model routines via the ECIS06 code [27,28]. Concerning direct reaction channels, spherical optical model calculations were performed, and, in order to account for the correlation between the incident and exit channels in elastic scattering, width fluctuation corrections were activated implementing the model of Hofmann, Richert, Tepel and Weidenmuller (HRTW) [29] up to an incident neutron energy of 3 MeV. γ emission, which is important for nuclear deexcitation in the low energy range, was described by using modified Lorentzian (MLO1) γ-ray strength functions by Plujko [30], with parameters available in the RIPL-3 database [31]. All the available in RIPL-3 neutron optical model potentials [32–44] were tested, but the one introduced by Wilmore *et al.* [35] was finally chosen, for yielding the most satisfying results on the simultaneous reproduction of the ^{191}Ir$(n, 2n)^{190}$Ir$^{g+m1+0.086\,m2}$ and ^{191}Ir$(n, 2n)^{190}$Ir^{m2} reaction cross sections. Concerning the optical model parameters for the outgoing protons, the data by Koning *et al.* [42] were adopted, while parameters obtained by Avrigeanu *et al.* [45] were used for the outgoing alphas. Furthermore, the classical exciton model [46] was implemented by means of the PCROSS code [12], which is included in EMPIRE, to account for the pre-equilibrium emission mechanism. By using the aforementioned parametrization, apart from the two measured $(n, 2n)$ reaction channels, a quite satisfactory reproduction of the cross section of the $(n, 3n)$, (n, p), (n, α), and $(n,$ total) channels was also achieved (see Fig. 7).

Concerning cross section theoretical calculations with the TALYS 1.8 code, the basic keywords used in the input file are shown in Table VI. The nuclear level densities were described according to the generalized superfluid model (GSM), whereas the asymptotic level density parameters ($\tilde{\alpha}$) for the ^{192}Ir, ^{191}Ir, ^{190}Ir, and ^{189}Ir nuclei were explicitly declared in order to take the values from literature [47] as mentioned in Ref. [7]. Moreover, direct inelastic scattering was treated by distorted wave Born approximation (DWBA), whereas width fluctuation corrections were included for neutrons up to 3 MeV using again the Hofmann-Richert-Tepel-Weidenmüller (HRTW) model. γ-ray transitions with a multipolarity up to 4 were taken into account with strength functions calculated by the Kopecky-Uhl generalized Lorentzian model. Regarding the optical model potential for outgoing neutrons, the default option of TALYS was used, implementing the global parametrization of Koning and Delaroche [42], while for α particles the parameters by Avrigeanu *et al.* [48] were adopted. Concerning preequilibrium emission, the exciton model was assumed and the transition rates between exciton states were approached numerically with the optical model for collision probability. In order to fairly reproduce the cross section of the second isomeric state, the spin distribution for the preequilibrium population of the residual nuclei was chosen based on the particle-hole state densities and the spin cutoff parameter was multiplied by a factor of 0.7. Furthermore, the spin cutoff parameter for the ground state level densities was described by means of the following model:

$$\sigma^2 = c\sqrt{\frac{U}{\alpha}}, \tag{4}$$

where c is a constant, α is the level density parameter determined either by experimental information or by global systematics, and U is the excitation energy subtracting an empirical parameter related to the pairing energy ($U = E - \Delta$). In addition, for the stripping and pickup preequilibrium processes of outgoing α particles a scale factor of 2 was used [2].

VII. RESULTS AND DISCUSSION

The cross section of the ^{191}Ir$(n, 2n)$ reaction for two experimental channels, resulting in the ^{190}Ir^{m2} and ^{190}Ir$^{g+m1+0.086\,m2}$ residual nuclei respectively, as well as the ^{191}Ir$(n, 3n)$ reaction cross section were measured at incident neutron beam energies ranging from 15.3 to 20.9 MeV, and the results are presented in Figs. 4–6. The new data points for the cross section of the second metastable state (Fig. 4) result in a higher cross section compared to the majority of the previously existing datasets, while they agree only with the data introduced by Bormann *et al.* [10]. Moreover, they strongly indicate that the centroid of the cross section curve is formed at ∼17 MeV. Regarding the ^{191}Ir$(n, 2n)^{190}$Ir$^{g+m1+0.086\,m2}$ reaction cross section, the experimental results (Fig. 5) follow the general trend pointed out by previous data points over the whole energy range. Especially the new experimental data point at 15.3 MeV reveals that the cross section plateau lies near the lowest experimental data existing in literature, meaning close to the central values given by Filatenkov *et al.* [8], Konno *et al.* [49], and Temperley *et al.* [3] and not so close to the central values obtained

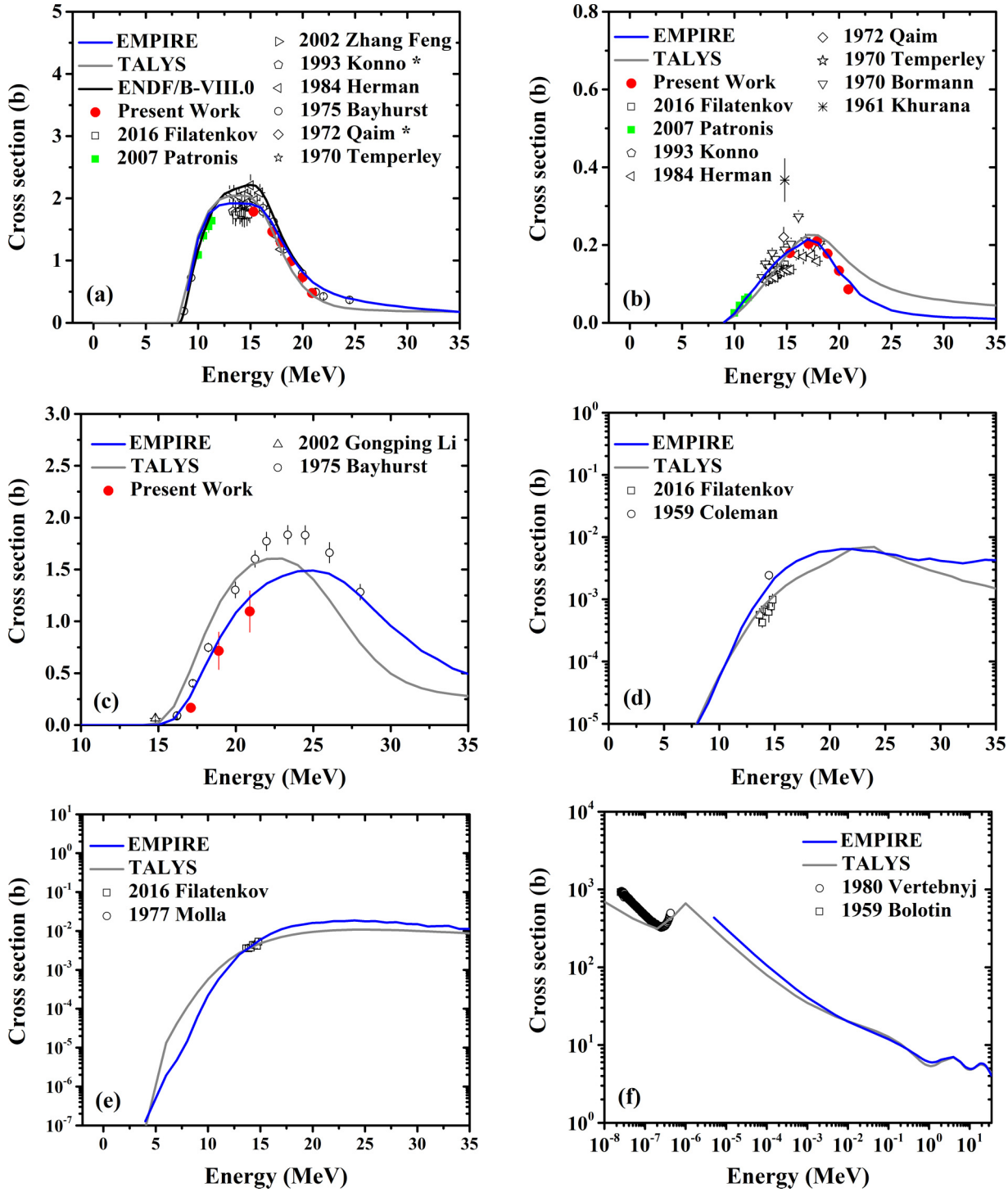

FIG. 7. Cross sections of six reaction channels for the $n + {}^{191}\mathrm{Ir}$ interaction. The experimental results of this work for the $(n, 2n)$ channels are presented along with existing data in literature [9] and theoretical calculations obtained with EMPIRE 3.2.2 and TALYS 1.8 codes. Each reaction channel is shown separately: (a) ${}^{191}\mathrm{Ir}(n, 2n){}^{190}\mathrm{Ir}^{g+m1+0.086\,m2}$, (b) ${}^{191}\mathrm{Ir}(n, 2n){}^{196}\mathrm{Ir}^{m2}$, (c) ${}^{191}\mathrm{Ir}(n, 3n){}^{189}\mathrm{Ir}$, (d) ${}^{191}\mathrm{Ir}(n, \alpha){}^{188}\mathrm{Re}$, (e) ${}^{191}\mathrm{Ir}(n, p){}^{191}\mathrm{Os}$, and (f) ${}^{191}\mathrm{Ir}(n, \mathrm{total})$.

by Herman *et al.* [5], Bayhurst *et al.* [4], and Qaim *et al.* [50] (although some points of the latter datasets agree within errors with the present ones). Therefore, the cross section plateau also lies much lower than the mean value indicated by the ENDF/B-VIII.0 evaluation for the 11–18 MeV energy region. Concerning the ${}^{191}\mathrm{Ir}(n, 3n)$ reaction channel, only few measurements exist in literature [4,11] and the new points present significant discrepancies with them. It seems that the cross section is overestimated by the data of Bayhurst *et al.* [4], and furthermore it seems that the cross section curve starts to

TABLE VI. Basic keywords and the corresponding values used in the input file of the TALYS 1.8 code.

Keyword	Value
ldmodel	3
alimit	77 192 16.4
alimit	77 191 16.3
alimit	77 190 16.2
alimit	77 189 16.1
spherical	*n*
widthfluc	3
widthmode	2
gammax	4
strength	1
jlmomp	*n*
alphaomp	6
preequilibrium	*y*
preeqmode	3
preeqspin	3
rspincut	0.7
spincutmodel	2
cstrip	α 2

increase at slightly higher energies compared to ENFB/VIII.0 evaluation (Fig. 6).

The cross section theoretical calculation results obtained from EMPIRE 3.2.2 and TALYS 1.8 codes are presented in Fig. 7 along with the data points of the present work and already existing experimental datasets in literature [9]. The reproduction of the cross section is quite good for all the studied reaction channels. More specifically, in the case of the second isomeric state [Fig. 7(b)] both codes seem to describe well the trend of experimental data and the position of the cross section maximum. However, the EMPIRE (blue) curve reproduces the cross section slightly better than TALYS (grey) curve in both low (near threshold) and high energy regions. It seems that if there was the flexibility of a multiplication factor in the preequilibrium mechanism contribution in the TALYS code, it would be possible to describe much better the right tail of the cross section curve. It should be noted that the reproduction of this reaction channel alone was better without taking into account the contribution of preequilibrium emission (when using the TALYS code). But this scenario could not be accepted, first because it is not physically expected and second because there was an additional constraint introduced by the goal of simultaneously describing the two measured $(n, 2n)$ channels, and it seemed that when the result for the $m2$ level improved, the result for the cross section of the sum of the levels $(g + m1 + 0.086\,m2)$ presented increased deviations. Regarding the cross section of the ^{191}Ir$(n, 2n)^{190}$Ir$^{g+m1+0.086\,m2}$ reaction channel [Fig. 7(a)], both curves are in very good agreement with experimental data, while TALYS for neutron energies above 15 MeV seems to slightly overestimate the $(n, 3n)$ channel [Fig. 7(c)] at the expense of the $(n, 2n)$ one. It should be noted that the ^{191}Ir$(n, 2n)^{190}$Ir$^{g+m1+0.086\,m2}$ cross section data could be well reproduced by many combinations of optical and level density models using both codes. The strong constraint for the selection of the final combination of the parameters turned out to be the simultaneous reproduction of the cross sections for both ground and second isomeric states.

At this point it should be mentioned that the same behavior concerning the neutron evaporation was observed when cross section theoretical calculations were carried out by using the EMPIRE 3.2.2 and TALYS 1.8 codes for the interaction of neutrons with the neighboring ^{197}Au nucleus [51]. It is also worth mentioning that in those cross section theoretical calculations performed with the EMPIRE code for the $n + {}^{197}_{79}$Au system [51], the same optical model parameters (Wilmore *et al.* [35]) as those used in the present work for the $n + {}^{191}_{77}$Ir system, as well as EGSM level densities, were chosen for yielding the most satisfactory results. These similarities in the theoretical parametrization are not that surprising since both nuclei belong in the transitional region from well deformed to spherical nuclei near the $Z = 82$ shell closure (Os–Pb region), where high spin intruder configurations result in high spin isomeric states unable to communicate with neighboring states [52]. In the case of the ^{197}Au$(n, 2n)$ reaction, the residual nucleus ^{196}Au can be produced either in its ground state $(g, 4^-)$ or in a high spin isomeric state $(m2, 12^-)$ which can be attributed to the configuration $\pi h11/2 \otimes \nu i13/2$. In a similar way, in the case of the ^{191}Ir$(n, 2n)$ reaction, the residual nucleus ^{190}Ir can be produced either in its ground state $(g, 4^-)$ or in its high spin isomeric state $(m2, 11^-)$ attributed to the $\pi h11/2 \otimes \nu 11/2$ configuration [53]. By using almost the same parametrization, both ^{197}Au$(n, 2n)^{196}$Au^{m2} and ^{191}Ir$(n, 2n)^{190}$Ir^{m2} reaction cross sections reproduced very well the behavior of the experimental data, for both near threshold and higher energies, as well as for middle energies in the plateau region. Furthermore, it is observed that the cross section maximum in the two reactions is ∼200 mb and is centered around 17 MeV, as revealed by both theoretical calculations and experimental data. In addition, it may be worth mentioning that in theoretical calculations with EMPIRE code for both the $n + {}^{196}$Au and $n + {}^{191}$Ir systems, the $(n, 2n)$ cross section for the ground state is slightly and systematically overestimated over the whole studied energy region.

Concerning the $(n, 3n)$ reaction channel, the results obtained from both codes seem to underestimate the cross section compared to the data by Bayhurst *et al.* [4], but compared to the present work, especially the results of EMPIRE code present a very good agreement. Furthermore, concerning the charged particle reaction channels [see Figs. 7(d) and 7(e)], both codes seem to reproduce in a quite satisfactory manner the cross sections, although there is a certain lack of experimental data. In addition, results of both codes for the total reaction cross section [Fig. 7(f)] agree well with each other, but for this case there is a certain need for experimental cross section measurements for energies above 10^{-6} MeV. Cross section data for the (n, total) reaction over a wide energy range exist in literature but only for the case of natural Ir and not for each isotope separately [9,54].

VIII. CONCLUSIONS

The ^{191}Ir$(n, 2n)^{190}$Ir$^{g+m1+0.086\,m2}$, ^{191}Ir$(n, 2n)^{190}$Ir^{m2}, and ^{191}Ir$(n, 3n)^{190}$Ir reaction cross sections have been measured at incident neutron energies covering the range between 15.3

and 20.9 MeV, relative to the ^{27}Al$(n,\alpha)^{24}$Na reaction reference cross section. The irradiations were performed at the 5.5 MV Tandem T11/25 Accelerator Laboratory of NCSR "Demokritos" in Athens, by means of the activation technique. The experimental results for the cross section of the ^{191}Ir$(n,2n)^{190}$Ir$^{g+m1+0.086\,m2}$ reaction are in good agreement with previously existing data and indicate that the maximum value in which the plateau region lies is about 19% lower than the ENDF/B-VIII.0 evaluation value, whereas for the ^{191}Ir$(n,2n)^{190}$Ir^{m2} reaction the new data points clearly reveal the shape of the cross section curve above 15 MeV and show that its maximum plateau is centered around 17 MeV. The new data points for the cross section of the ^{191}Ir$(n,3n)^{189}$Ir reaction present significant discrepancies with both previous existing datasets and the ENDF/B-VIII.0 evaluation and reveal that the cross section is much lower and starts to increase at slightly higher energies. Furthermore, theoretical cross section calculations have been carried out in the energy range 10^{-8}–35 MeV, including the experimental results obtained in the present work along with data from literature for three additional reaction channels by means of the EMPIRE 3.2.2 and TALYS 1.8 nuclear model codes. Both codes reproduced fairly well all the studied reaction channels, including the isomer production, while the observation that a similar combination of parameters had also been used in cross section theoretical calculations performed for neutron interactions on the neighboring ^{197}Au nucleus [51] provides an encouraging confirmation of how successfully the theoretical models can reproduce the experimental results in this mass region.

ACKNOWLEDGMENTS

This research is implemented through an IKY scholarships program which was financed through the action "Funding scholarship programme for second cycle post-graduate studies" in the framework of the Operational Programme "Human Resources Development Program, Education and Lifelong Learning", 2014–2020, and was co-financed by the European Union (European Social Fund, ESF) and Greek national funds. Furthermore, the authors would like to acknowledge the support of this work by the project "CALIBRA/EYIE" (MIS 5002799) which is implemented under the Action "Reinforcement of the Research and Innovation Infrastructure", funded by the Operational Programme "Competitiveness, Entrepreneurship and Innovation" (NSRF 2014-2020) and cofinanced by Greece and the European Union (European Regional Development Fund). Last but not least, the authors would like to acknowledge the assistance of the accelerator staff at NCSR "Demokritos".

[1] M. B. Chadwick *et al.*, Evaluated iridium, yttrium, and thulium cross sections and integral validation against critical assembly and Bethe sphere measurements, Nucl. Data Sheets **108**, 2716 (2007).
[2] N. Dzysiuk and A. Koning, Improving activation cross section data with TALYS, EPJ Web Conf. **146**, 02047 (2017).
[3] J. K. Temperley and D. E. Barnes, Neutron Activation Cross Sections for Some Isotopes of Ruthenium, Palladium, Indium, Tin, and Iridium, Ballistic Research Laboratory Report No. 1491, 1970 (unpublished).
[4] B. P. Bayhurst *et al.*, Cross sections for (n,xn) reactions between 7.5 and 28 MeV, Phys. Rev. C **12**, 451 (1975).
[5] M. Herman *et al.*, Statistical multi-step compound emission in (n, 2n) reactions, Nucl. Phys. A **430**, 69-83 (1984).
[6] Zhang Feng *et al.*, Measurement of cross sections for the ^{185}Re$(n,2n)^{184g,m}$Re and ^{191}Ir$(n,2n)^{190}$Ir reactions by 14 MeV neutrons, High Energy Phys. Nucl. Phys. **26**, 678 (2002).
[7] N. Patronis, C. T. Papadopoulos, S. Galanopoulos, M. Kokkoris, G. Perdikakis, R. Vlastou, A. Lagoyannis, and S. Harissopulos, Activation cross section and isomeric cross-section ratio for the $(n,2n)$ reaction on ^{191}Ir, Phys. Rev. C **75**, 034607 (2007).
[8] A. A. Filatenkov, Neutron Activation Cross Sections Measured at KRI in Neutron Energy Region 13.4–14.9 MeV, INDC International Nuclear Data Committee, IAEA Report No. INDC(CCP)-0460 Rev, 2016 (unpublished).
[9] EXFOR, http://www.nndc.bnl.gov/exfor/exfor.htm
[10] M. Bormann *et al.*, Total cross sections and isomeric cross-section ratios for (n, 2n) reactions in the energy region 12–18 MeV, Nucl. Phys. A **157**, 481 (1970).
[11] G. Li *et al.*, Cross section measurements for $(n,3n)$ reactions induced by 14.8 MeV neutrons, Appl. Radiat. Isot. **56**, 731 (2002).
[12] M. Herman *et al.*, EMPIRE: Nuclear reaction model code system for data evaluation, Nucl. Data Sheets **108**, 2655 (2007).
[13] A. Koning, S. Hilaire, and S. Goriely, TALYS-1.8, http://www.talys.eu/fileadmin/talys/user/docs/talys1.8.pdf 2015.
[14] NNDC, https://www.nndc.bnl.gov/
[15] S. Cowell *et al.*, Evaluation of iridium (n, xn) reactions, in *International Conference on Nuclear Data for Science and Technology ND2007* (EDP Sciences, Les Ulis, France, 2007).
[16] P. E. Garrett *et al.*, Long-lived isomers in ^{190}Ir, Nucl. Phys. A **11**, 68 (1996).
[17] A. Kalamara, R. Vlastou, M. Kokkoris, M. Diakaki, A. Tsinganis, N. Patronis, M. Axiotis, and A. Lagoyannis, Investigation of the ^{241}Am$(n,2n)^{240}$Am cross section, Phys. Rev. C **93**, 014610 (2016).
[18] R. Vlastou *et al.*, Neutron induced reactions with the 17 MeV facility at the Athens Tandem Accelerator NCSR "Demokritos", Phys. Proc. **66**, 425 (2015).
[19] X-5 Monte Carlo team, MCNP-A General Monte Carlo N-ParticleTransport Code, version 5, Volume I-III, LA-UR-03-1987, LA-CP-03 0245, and LA-CP-03-0284, April, 2003.
[20] ENDF, https://www-nds.iaea.org/exfor/endf.htm
[21] N. Otuka *et al.*, Uncertainty propagation in activation cross section measurements, Radiat. Phys. Chem. **140**, 502 (2017).
[22] W. Mannhart, A Small Guide to Generating Covariances of Experimental Data, IAEA Report No. INDC(NDS)-0588 Rev., 2013.
[23] https://www-nds.iaea.org/index-meeting-crp/EmpireWorkshop2013/downloadEmpire322win.htm
[24] http://www.talys.eu/download-talys/
[25] W. Hauser and H. Feshbach, The Inelastic Scattering of Neutrons, Phys. Rev. **87**, 366 (1952).

[26] A. D'Arrigo *et al.*, Semi-empirical determination of the shell correction temperature and spin dependence by means of nuclear fission, J. Phys. G **20**, 365 (1994).
[27] J. Raynal, Optical Model and Coupled-Channel Calculations in Nuclear Physics, IAEA Report No. IAEA-SMR-9/8, 1970 (unpublished).
[28] J. Raynal, Computing as a language of physics, IAEA-ICTP International Seminar Course, Italy, 1971.
[29] H. M. Hofmann *et al.*, Direct reactions and Hauser-Feshbach theory, Ann. Phys. (NY) **90**, 403 (1975).
[30] V. A. Plujko, A new closed-form thermodynamic approach for radiative strength functions, Acta Phys. Pol. B **31**, 435 (2000).
[31] R. Capote *et al.*, https://www-nds.iaea.org/RIPL-3/, 2009.
[32] F. D. Becchetti Jr. and G. W. Greenlees, Nucleon-Nucleus Optical-Model Parameters, $A > 40$, $E < 50$ MeV, Phys. Rev. **182**, 1190 (1969).
[33] J. C. Ferrer, J. D. Carlson, and J. Rapaport, Neutron elastic scattering at 11 MeV and the isospin dependence of the neutron-nucleus optical potential, Nucl. Phys. A **275**, 325 (1977).
[34] P. A. Moldauer, Optical model of low energy neutron interactions with spherical nuclei, Nucl. Phys. **47**, 65 (1963).
[35] D. Wilmore and P. E. Hodgson, The calculation of neutron cross-sections from optical potentials, Nucl. Phys. **55**, 673 (1964).
[36] O. Bersillon and N. Cindro, in *Fifth International Symposium On Interactions of Fast Neutrons with Nuclei, Gaussig, 1975* (unpublished).
[37] C. A. Engelbrecht and H. Fiedeldey, Nonlocal potentials and the energy dependence of the optical model for neutrons, Ann. Phys. (NY) **42**, 262 (1967).
[38] D. G. Madland, Nucleon Nucleus Optical Model up to 200 MeV, OECD/NEA Proceedings of a Specialist Meeting, Paris, 1997 (unpublished), p. 129.
[39] R. Macklin and P. G. Young, Neutron capture cross sections of rhenium from 3 to 1900 keV, Nucl. Sci. Eng. **97**, 239 (1987).
[40] R. L. Varner *et al.*, A global nucleon optical model potential, Phys. Rep. **201**, 57 (1991).
[41] R. L. Walter and P. P. Guss, A global optical model for neutron scattering for a > 53 and 10 MeV < E < 80 MeV, Radiat. Eff. **95**, 73 (1986).
[42] A. J. Koning and J. P. Delaroche, Local and global nucleon optical models from 1 keV to 200 MeV, Nucl. Phys. A **713**, 231 (2003).
[43] B. Morillon and P. Romain, Dispersive and global spherical optical model with a local energy approximation for the scattering of neutrons by nuclei from 1 keV to 200 MeV, Phys. Rev. C **70**, 014601 (2004); Bound single-particle states for neutrons from a global spherical optical model, **74**, 014601 (2006).
[44] B. Morillon and P. Romain, Bound single-particle states and scattering of nucleons on spherical nuclei with a global optical model, Phys. Rev. C **76**, 044601 (2007).
[45] V. Avrigeanu, P. E. Hodgson, and M. Avrigeanu, Global optical potentials for emitted alpha particles, Phys. Rev. C **49**, 2136 (1994).
[46] J. J. Griffin, Statistical Model of Intermediate Structure, Phys. Rev. Lett. **17**, 478 (1966).
[47] T. Belgya *et al.*, IAEA-TECDOC-1506, https://www-nds.iaea.org/RIPL-2/, 2006.
[48] V. Avrigeanu, M. Avrigeanu, and C. Manailescu, Further explorations of the α-particle optical model potential at low energies for the mass range $A \approx 45$–209, Phys. Rev. C **90**, 044612 (2014).
[49] C. Konno *et al.*, Activation Cross Section Measurements at Neutron Energy from 13.3 to 14.9 MeV, Japan Atomic Energy Research Institute Report No. JAERI-1329, 1993 (unpublished).
[50] S. M. Qaim, Activation cross sections, isomeric cross-section ratios and systematics of (n, $2n$) Reactions at 14–15 MeV, Nucl. Phys. A **185**, 614 (1972).
[51] A. Kalamara, R. Vlastou, M. Kokkoris, N. G. Nicolis, N. Patronis, M. Serris, V. Michalopoulou, A. Stamatopoulos, A. Lagoyannis, and S. Harissopulos, ^{197}Au(n, $2n$) reaction cross section in the 15–21 MeV energy range, Phys. Rev. C **97**, 034615 (2018).
[52] A. Tsinganis, M. Diakaki, M. Kokkoris, A. Lagoyannis, E. Mara, C. T. Papadopoulos, and R. Vlastou, Isomeric cross section of the ^{197}Au(n, $2n$) reaction, Phys. Rev. C **83**, 024609 (2011).
[53] Y. P. Gangrsky *et al.*, Isomeric ratios in reactions induced by gamma rays and fast neutrons in the isotopes of Re, Ir, and Au, Phys. At. Nucl. **67**, 1227 (2004).
[54] Y. D. Lee and Y. O. Lee, Neutron induced cross section data for Ir-191 and Ir-193, Nucl. Eng. Technol. **38**, 803 (2006).